$x_{t,ik}^{(j)} = \frac{\partial x_{ij}}{\partial t_k}$; $y_{t,ik}^{(j)} = \frac{\partial y_{ij}}{\partial t_k}$

$\mathbf{X}_v^{(j)}$, $\mathbf{Y}_v^{(j)}$ = flow rate dependence matrices for liquid and vapor composition. The volumes of $\mathbf{X}_v^{(j)}$ and $\mathbf{Y}_v^{(j)}$ are calculated from Equation (38)

$x_{v,ik}^{(j)} = \frac{\partial x_{ij}}{\partial v_k^*}$

$y_{v,ik}^{(j)} = \frac{\partial y_{ij}}{\partial v_k^*}$

$\mathbf{Z}^j = \mathbf{L} + \mathbf{V}\ \mathbf{K}^j$

Greek Letters

Φ = correction matrix used to calculate temperature and flow rate corrections

Ψ = Jacobian form of the correction matrix

$\psi_{ij} = \frac{\partial \lambda_i}{\partial \delta_j}$

$\Delta = \begin{bmatrix} C_t \\ C_v \end{bmatrix} = (\delta_i)$

$\Lambda = \begin{bmatrix} D_m \\ D_e \end{bmatrix} = (\lambda_i)$

LITERATURE CITED

1. Friday, J. R., and B. D. Smith, *A.I.Ch.E. J.*, **10**, 698-706 (1964).
2. Henrici, Peter, "Elements of Numerical Analysis," Chap. V, Wiley, New York (1964).
3. Amundson, N. R., and A. J. Pontinen, *Ind. Eng. Chem.*, **50**, 730-736 (1958).
4. ————, and J. W. Tierney, *A.I.Ch.E. J.*, **5**, 295-300 (1959).
5. Bruno, Joseph A., M.S. thesis, Univ. Pittsburgh (1966).
6. Hanson, D. N., J. H. Duffin, and G. F. Sommerville, "Computation of Multistage Separation Processes," p. 347, Reinhold, New York (1962).
7. Varga, R. S., "Matrix Iterative Analysis," p. 194, Prentice-Hall, Englewood Cliffs, N. J. (1962).
8. Strand, C. P., *Chem. Eng. Progr.*, **59**, No. 4, 58-64 (1963).

Manuscript received July 28, 1965; revision received September 9, 1966; paper accepted September 30, 1966.

Local and Macroscopic Transport from a 1.5-In. Cylinder in a Turbulent Air Stream

T. R. GALLOWAY and B. H. SAGE

California Institute of Technology, Pasadena, California

The local and macroscopic thermal transfer coefficients were experimentally investigated for a 1.5-in. copper cylinder located in a transverse flowing turbulent air stream. Measurements of local transport and pressure coefficient were made throughout the entire perimeter of the cylinder. The Reynolds number was varied from 2,600 to 86,000 and the free-stream turbulence from 0.013 to 0.25. The estimated integral turbulence scale was found to vary from 0.3 to 0.5 in. over the range of conditions of flow investigated. The local transfer coefficient near stagnation increased 35% as a result of an increase in turbulence over the range indicated. Displacements of the locus of separation with varying Reynolds numbers and turbulence level were found.

The effects of free-stream turbulence on the local thermal transfer from a blunt body are particularly interesting in revealing the mechanism of transport. These experimental studies are directed, in part, to an understanding of the behavior of the wake. It is the purpose of this discussion to present experimental results concerning the effect of free-stream turbulence on the local transport from a cylinder.

THEORY AT STAGNATION

One of the most significant and extensive contributions to local transport, both theoretically as well as experimentally, was the work of Frössling (*1*). He suspended liquid drops over an air jet and measured the change in radius by photomicrography. The drop radii varied from 0.1 to 0.9 mm. and the air velocity from 0.2 to 7 m./sec., corresponding to a Reynolds number as defined in the Notation from 2 to 800 for the evaporation of nitrobenzene, aniline, and water. Local convective rates were determined by measuring the pointwise variation in the radius of a solid naphthalene sphere in an air jet stream. Frössling (*1*) showed theoretically that

$$N_{Nu} = 2(1 + k\, N_{Re}^{1/2}) \qquad (1)$$

where his k was dependent only on the Prandtl number,

and for macroscopic transport could be represented approximately by

$$k = 0.276\, N_{Pr}^{1/3} \tag{2}$$

His theoretical analysis of local transport still is worthy of review. He considered the term k in Equation (1) to be angularly dependent, referring to the contribution in parentheses in Equation (1) as the "windfactor." The theoretical analysis (*1*) showed that only the coefficient of Equation (2) was dependent upon angle up to the locus of separation. This behavior suggested the utility of the quotient

$$N_{Fs} = \frac{N_{Nu} - 2}{N_{Re}^{1/2}\, N_{Pr}^{1/3}} \tag{3}$$

Such a quantity for spheres has been identified as the Frössling number. The corresponding number for cylinders with a large enough length-to-diameter ratio to permit a two-dimensional treatment may be stated as follows:

$$N_{Fs} = \frac{N_{Nu}}{N_{Re}^{1/2}\, N_{Pr}^{1/3}} \tag{4}$$

and yields a value of 1.05 at stagnation from analysis. Squire found 1.11 by an alternate analysis (*2*) and 1.02 by an integral approach (*3*). Korobkin (*4*) has reviewed various other analyses for spheres and cylinders at stagnation.

THE FRÖSSLING NUMBER AND TURBULENCE

Increases in heat transfer with turbulence were observed as early as 1925 (*5*). Subsequent to that time, a number of systematic studies of turbulence have been made (*6* to *14*). Churchill and co-workers (*15, 16*) carried out heat transfer measurements on cylinders and correlated the results of numerous other investigators. Perkins and Leppert (*17*) studied forced thermal convection from cylinders to a stream of water and to ethylene glycol up to a Reynolds number of 100,000, and varied the Prandtl number from 1 to 300. The fractional turbulence level was 0.0108. Their results reflect behavior characteristic of transport in the wake involving gaseous streams. Richardson (*18, 19*) has reviewed a substantial amount of data and concludes that the Reynolds number dependence in the laminar portion and in the turbulent wake portion can be represented separately. Grafton (*20*) concludes that in the laminar region the local Frössling number is independent of the Reynolds number, whereas in the wake it is not.

In the examination of the data for both cylinders and spheres, it was found that the Frössling number is a useful transport parameter for both thermal and material transfer from blunt bodies. The Frössling number appears to be a complicated function of angle measured from stagnation, Reynolds number, turbulence level, and perhaps of scale of turbulence, as well as of the molecular physical properties of the fluid. From semitheoretical stochastic considerations concerning the effects of eddy transport induced in the laminar boundary layer from the external turbulent free stream, the following form of an empirical expression for either macroscopic or local Frössling number appears to be useful:

$$N_{Fs_\infty} = A\left(\frac{\nu_\infty}{\nu_i}\right)^{0.16} + \left[B\left(\frac{\alpha_t}{\alpha_t + C}\right) + D\right] N_{Re_\infty}^{1/2} N_{Pr_{m,\infty}}^{1/6} \tag{5}$$

An analogous equation may be written for material transfer in situations where the Lewis number is near unity, and the Frössling numbers for thermal and material transfer are equivalent. The analogy breaks down at material transfer rates where the momentum velocity normal to the interface becomes important. The effect of composition variations is as yet unknown.

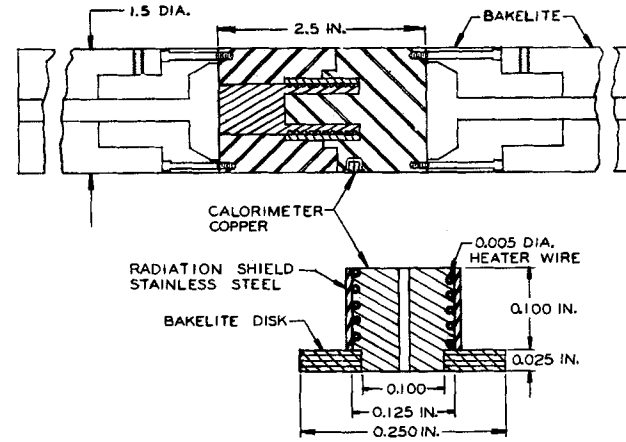

Fig. 1. 1.5-inch copper cylinder and calorimeter.

EXPERIMENTAL APPARATUS

In Figure 1 is shown the 1.5-in. copper cylinder equipped with a small solid copper calorimeter 0.100 in. in diameter at the surface, supported by a thin Bakelite disk. The lower portion of the figure shows an enlargement of the calorimeter and disk. Advance wire 0.005 in. in diameter was wound into spiral grooves within the calorimeter. A stainless steel radiation shield was mounted on the outside of the calorimeter which was fitted into a small well in the main cylinder. In operation, the calorimeter heater current was adjusted by voltage dividers until the temperature difference between the calorimeter surface and the surface of the copper cylinder was reduced to less

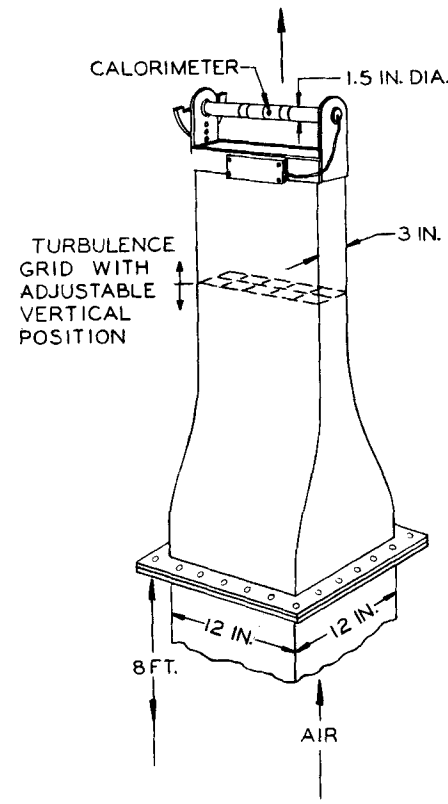

Fig. 2. Arrangement of cylinder and duct.

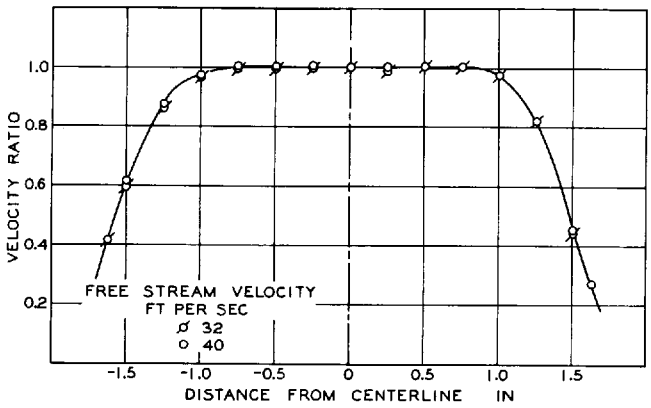

Fig. 3. Velocity ratio as function of position.

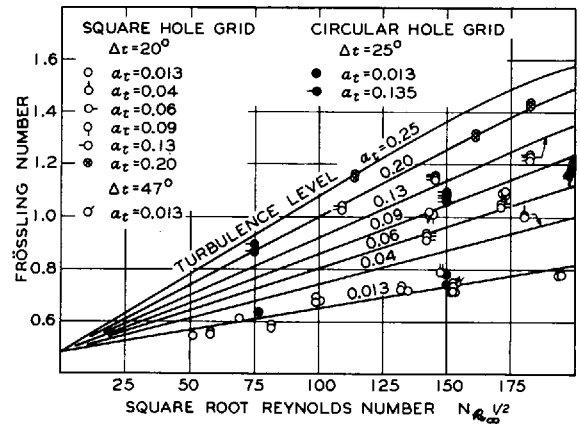

Fig. 4. Effect of turbulence on macroscopic thermal transport.

than 0.02°F. The measurements of temperature differences were made, using the indications of a copper-constantan thermocouple connected to a galvanometer with a sensitivity of 50 nanovolts/mm. Temperatures were measured in the calorimeter and at a number of locations in the cylinder. The local thermal transfer coefficient was obtained from local values of the measured thermal flux and temperature difference, while the macroscopic measurements were made using the total cylinder thermal flux and average temperature difference. Thermal loss from the calorimeter as a function of temperature difference was measured at different angles in situ with no flow. The measured loss was subtracted directly from the flux as a correction.

The cylinder was mounted at the top of a 3 in. by 12 in. rectangular duct as shown in Figure 2. An 8-ft. long 12 in. by 12 in. damping section was used, which was then reduced to the section size of the rectangular jet. Such a reduction in section decreased the longitudinal turbulence level in the emerging jet to 0.013. Damping screens of 0.1 in. square mesh were employed before and after the damping section. Various turbulence levels were generated, as shown in Figure 2, by varying the downstream distance of the cylinder from both a "punched plate grid" which was constructed similar to that described by van der Hegge Zijnen as his grid "27/7" (*21*), and from a "circular-hole grid" patterned after Davis (*22, 23*). The measurements of van der Hegge Zijnen and Davis were used to establish the longitudinal turbulence level and to estimate the integral scale as a function of downstream position from the grid. The evaluation of the level of turbulence as a function of downstream position from a grid or punched plate is subject to some uncertainty, and the authors have indicated this uncertainty by the designation *apparent level of longitudinal turbulence,* hereinafter referred to as *level of turbulence.* The Reynolds number was evaluated from the measured macroscopic velocity at a point 0.5 in. upstream of stagnation locus of the cylinder. The time-average velocity across the exit of the working section remained relatively flat for the conditions investigated as shown in Figure 3. It should be recognized that the cylinder located at the exit of the duct undoubtedly was subjected to somewhat different flow conditions than if it had been immersed in a flowing stream of large cross section relative to the diameter of the cylinder. The prediction of these effects is difficult, just as the blockage effect in wind tunnels. However, the pressure coefficient was measured as a function of angle from stagnation in nearly all cases of study of the local thermal transport.

EXPERIMENTAL RESULTS

The measurements of macroscopic thermal transport from the 1.5-in. cylinder are recorded in Table 1, and Figure 4 depicts the Frössling number as a function of the Reynolds number with level of turbulence as a parameter. The empirical coefficients in Equation (5) for the macroscopic Frössling number in subcritical flow were evaluated by nonlinear regression techniques by use of the data in Table 1 and are

$$A = 0.4763 \qquad C = 0.1300$$
$$B = 0.007162 \qquad D = 0.001226$$

The standard error of estimate of experimental points from the curves which are based on Equation (5) and shown in Figure 4 was 3.39%. The average error was 0.11% and the experimental reproducibility was 0.9%. Throughout the measurements recorded in Table 1, the integral turbulence scale varied from 0.3 to 0.5 in. The scale of the turbulence was estimated from the geometry of the grid employed and the measurements of van der Hegge Zijnen (*21*).

Figure 5 shows the macroscopic Frössling number for a number of investigators (*7* to *11, 13, 14, 17, 21, 24, 25*), using the correction factor ν_∞/ν_i for the variations in the kinematic viscosity in the boundary flow. It should be

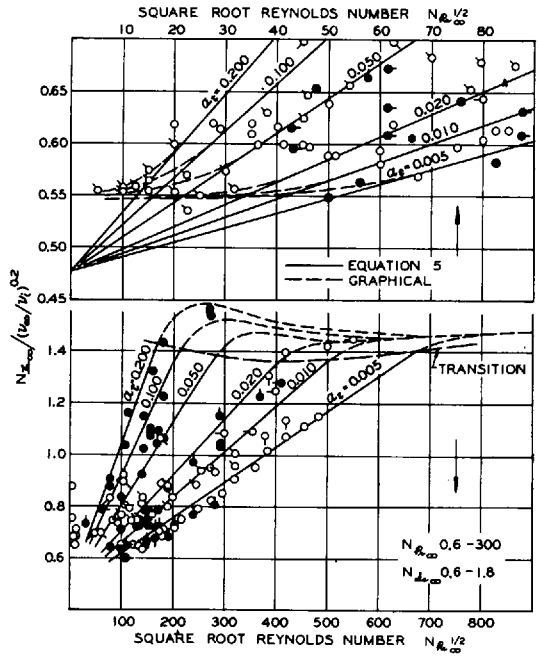

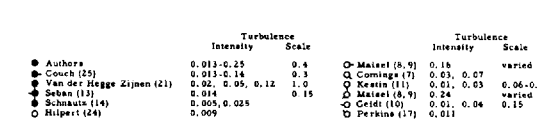

Fig. 5. Macroscopic Frössling number from several investigators.

TABLE 1. EXPERIMENTAL RESULTS FOR MACROSCOPIC THERMAL TRANSPORT

Test No.	Reynolds No.	Level of turbulence*	Temperature, °F. Air stream	Temperature, °F. Interface	Viscosity ratio†	Total thermal flux, B.t.u./sec.	Nusselt No.	Frössling No.‡
			Square hole grid (*21*)					
919	2667	0.013	90.62	103.17	0.9623	0.890×10^{-3}	25.29	0.5499
918	3382	0.013	93.07	108.44	0.9839	1.256	29.03	0.5604
917	4879	0.013	95.03	112.27	0.9481	1.879	38.83	0.6244
916	6706	0.013	94.14	113.33	0.9434	2.307	42.66	0.5851
915	10406	0.013	92.78	109.94	0.9489	2.938	60.87	0.6868
936	11966	0.222	84.08	106.25	0.9334	6.204	100.98	1.0354
935	13147	0.256	85.05	106.73	0.9349	7.148	118.68	1.1609
913	17570	0.013	92.30	103.90	0.9654	2.816	86.37	0.7312
910	18254	0.013	82.90	105.80	0.9316	5.523	87.58	0.7277
929	20364	0.090	88.91	104.98	0.9516	5.892	131.19	1.0267
928	20365	0.060	88.42	106.09	0.9464	5.830	118.22	0.9296
930	21305	0.139	89.19	103.46	0.9577	5.977	149.99	1.1529
927	21893	0.046	87.71	107.37	0.9411	5.745	104.84	0.7949
932	23329	0.013	91.19	138.01	0.9655	13.400	102.02	0.7500
931	23403	0.013	90.16	110.39	0.9394	5.586	98.61	0.7234
934	25942	0.210	85.54	106.48	0.9370	11.065	190.08	1.3236
925	29483	0.052	85.76	102.44	0.9550	7.424	160.00	1.0456
924	29958	0.079	85.62	100.86	0.9544	7.166	169.13	1.0963
923	32536	0.041	87.86	104.09	0.9515	7.319	161.70	1.0059
926	33422	0.120	83.01	97.74	0.9549	8.155	200.08	1.2278
933	33456	0.188	84.75	103.28	0.9445	12.038	234.12	1.4361
914	38160	0.013	89.63	104.15	0.9564	5.382	136.88	0.7852
			Circular hole grid (*22, 23*)					
641	5791	0.013	99.06	128.99	0.9608		43.21	0.6280
642A	5677	0.135	99.02	126.72	0.9635		58.49	0.8723
642B	5673	0.135	99.06	125.95	0.9645		60.54	0.9032
643A	22676	0.135	99.44	123.86	0.9676		147.08	1.0975
643B	22678	0.135	99.40	123.94	0.9675		144.22	1.0761
643C	22675	0.135	99.40	123.94	0.9675		142.83	1.0658
643D	21678	0.135	99.31	123.73	0.9676		142.03	1.0839
644A	22527	0.013	99.36	130.80	0.9590		104.99	0.7860
644B	22519	0.013	99.53	132.23	0.9575		100.09	0.7495
644C	22465	0.013	99.61	132.05	0.9578		100.08	0.7503
645A	85967	0.013	99.40	122.62	0.9692		266.77	1.0224
645B	85967	0.013	99.40	122.62	0.9692		271.10	1.0390
646A	72557	0.135	99.57	116.68	0.9773		370.15	1.5441
646B	72557	0.135	99.57	116.68	0.9773		372.84	1.5554
646C	73924	0.135	99.57	116.68	0.9773		369.41	1.5267

* Level of longitudinal turbulence defined by

$$\alpha_t = [\overline{(u'_{xf})^2}]^{1/2}/U_\infty$$

The integral scale of turbulence was estimated (*21*) to vary from 0.3 to 0.5 in.

† Viscosity ratio defined by ν_∞/ν_{f_i}.

‡ Prandtl number used in calculations varied between 0.7060 and 0.7085 and between 0.7048 and 0.7049 for data taken with the square hole and circular hole grids, respectively.

recognized that such a correction is empirical, but it has been found to be useful in bringing together the large amount of experimental information for both gas and liquid phases shown in Figure 5. The solid curves for subcritical flow are based upon Equation (5) with the above coefficients, while the dashed curves were established by graphical methods. The lower portion of Figure 5 depicts the transport data from investigators who established and systematically varied the longitudinal free-stream turbulence level. The upper portion of the figure depicts data for the lower Reynolds numbers upon an enlarged scale. The data of Perkins (*17*) for thermal transfer with water and ethylene glycol and that of Hilpert (*24*) for air show the same trends as do the more limited data of Couch (*25*) for material transfer to an air stream at low levels of turbulence and low Reynolds numbers. These trends indicate that there is little change in the Frössling number with Reynolds number at low values of the latter quantity. The data available from investigators who did not systematically vary or report the turbulence level have been reviewed by Douglas and Churchill (*16*), and qualitatively the trends are comparable to those shown in Figure 5.

Recorded in Table 2 is the standard error of estimate of each set of experimental data from the curves shown in Figure 5, as well as the values of the average error for each source of experimental data. It is apparent that there is some bias between one set of measurements and another. In the lower part of the table is shown the overall value of the standard error of estimate of all the data when the effects of natural convection have been removed. The upper part of Figure 5 represents the transition to supercritical flows. The curves for supercritical flow were based on the data of Kestin (*11*), Giedt (*10*), and Seban (*13*), all of whom made a study of the transition to critical flow established from pressure distributions. Geidt (*10*) noted that the macroscopic Nusselt number was affected less by turbulence at the critical Reynolds number than in subcritical flow, owing to large decreases in the pressure coefficient in the wake corresponding to transition

TABLE 2. COMPARISON OF RESULTS FOR MACROSCOPIC THERMAL TRANSPORT

Reference	No. of points	Turbulence level* Minimum	Turbulence level* Maximum	Deviation Average†	Deviation Standard‡
This work	34	0.013	0.25	0.0270	0.0457
Comings (*7*)	4	0.03	0.07	0.0157	0.0198
Couch (*25*)	10	0.013	0.14	0.0567	0.0709
Giedt (*10*)	4	0.01	0.04	0.0882	0.122
Hilpert (24)	27	0.009		0.0659	0.0854
Kestin (*11*)	5	0.01	0.03	0.0378	0.0458
Maisel (8, 9)	4	0.24		0.129	0.135
Perkins (*17*)	37	0.011		0.093	0.155
Schnautz (*14*)	13	0.005	0.025	0.0431	0.0561
Seban (*13*)	1	0.014		0.0110	0.0110
Van der Hegge Zijnen (*21*)	3	0.02	0.12	0.102	0.106
Overall	142			0.0609	0.0775

* Level of longitudinal turbulence defined by

$$\alpha_t = [\overline{(u'_{zt})^2}]^{1/2}/U_\infty$$

The integral scale of turbulence was estimated (*21*) to vary from 0.3 to 0.5 in.

† Average deviation defined by

$$s = \frac{\sum_1^N \left| \{[N^*_{Fs_\infty}/(\nu_\infty/\nu_i)^{0.2}]_e - [N^*_{Fs_\infty}/(\nu_\infty/\nu_i)^{0.2}]_p\}/[N^*_{Fs_\infty}/(\nu_\infty/\nu_i)^{0.2}]_e \right|}{N}$$

‡ Standard error of estimate defined by

$$\sigma = \left\{ \frac{\sum_1^N [\{[N^*_{Fs_\infty}/(\nu_\infty/\nu_i)^{0.2}]_e - [N^*_{Fs_\infty}/(\nu_\infty/\nu_i)^{0.2}]_p\}/[N^*_{Fs_\infty}/(\nu_\infty/\nu_i)^{0.2}]_e]^2}{N-1} \right\}^{1/2}$$

of the laminar boundary flow to turbulent flow before separation. The behavior in the supercritical region shown by dashed curves represents the transition to critical flow resulting from elevated turbulence. Data taken under these flow conditions are recorded in Table 1. Such transitional behavior is typical of transport from spheres (*26, 27*). It should be noted that in the upper part of Figure 5 there is a tendency for the data to yield larger values of the Frössling number than would be predicted directly from Equation (5). This may result from the increasing

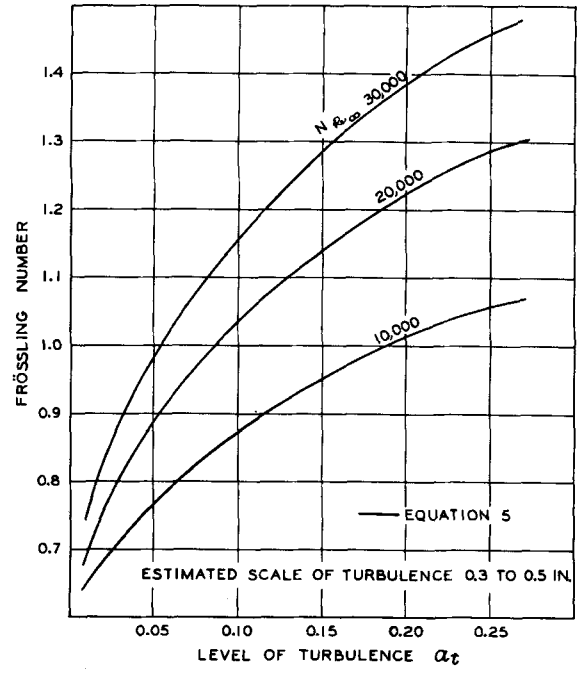

Fig. 6. Effect of level of turbulence upon macroscopic thermal transport.

importance of conduction and natural convection. It would be desirable, if possible, to correct the information shown in Figure 5 in an empirical way by deleting the natural convection and conduction from each of the experimental points. However, since there is no assurance that the natural convection and basic instabilities of the wake contribution can be simply superimposed on the forced convective transport, such action does not appear justified.

The effect of level of turbulence as predicted from Equation (5) is shown directly in Figure 6. As would be expected from earlier studies (*7, 10, 13, 20*), the effect of turbulence is most pronounced at the lower levels. Such trends are in contradistinction to the effect of turbulence upon transport from spheres. These curves do not converge to a single value in the limit of no turbulence, owing to the varying contribution of the wake.

TABLE 3. SAMPLE OF EXPERIMENTAL RESULTS FOR LOCAL THERMAL TRANSPORT

Angle,* deg.	Thermal flux,† B.t.u./sec.	Nusselt No.	Frössling No.	$N_{Nu_\infty}/N^*_{Nu_\infty}$	Thermal flux,† B.t.u./sec.	Nusselt No.	Frössling No.	$N_{Nu_\infty}/N^*_{Nu_\infty}$
		Test 919		Square hole grid (*21*)		Test 918		
0	2.947×10^{-6}	47.95	1.043	1.896	4.156×10^{-6}	55.27	1.067	1.904
20	2.920	47.54	1.034	1.880	4.012	53.36	1.030	1.838
40	2.597	42.28	0.919	1.672	3.534	47.00	0.907	1.619
60	1.818	29.59	0.643	1.170	2.525	33.59	0.648	1.157
80	0.622	10.12	0.219	0.400	0.581	7.72	0.149	0.266
85	0.315	5.11	0.111	0.202	0.174	2.32	0.0448	0.0779
90	0.108	3.29	0.0715	0.130	0.292	3.89	0.0751	0.134
100	0.369	5.99	0.130	0.237	0.835	11.09	0.214	0.382
110	0.838	13.63	0.296	0.539	1.206	16.02	0.309	0.552
120	0.887	14.44	0.314	0.571	1.191	15.85	0.306	0.546
130	0.928	15.10	0.328	0.597	1.244	16.55	0.319	0.570
140	1.059	17.22	0.374	0.681	1.557	20.70	0.399	0.713
160	1.339	21.80	0.474	0.862	2.024	26.91	0.519	0.927
180	1.586	25.82	0.561	1.021	2.483	33.01	0.637	1.137

* Angle measured from stagnation.
† The thermal flux is associated with an area of 0.077993 sq. ft.

With the use of the calorimeter described earlier, together with a small surface Pitot tube, the local thermal transport and pressure coefficients from the cylinder were established. A sample of the experimental results obtained is set forth in Table 3. The experimental data upon the local transport are available.† As an illustration of the complicated behavior encountered, the local transport expressed in terms of the Frössling number for Reynolds numbers of 12,000, 22,000, and 33,000 is shown in Figure 7 as a function of angle from stagnation, with the level of turbulence generated by the grid of van der Hegge Zijnen (*21*) as a parametric variable. The apparently anomalous behavior at the stagnation point for the higher turbulence levels and Reynolds numbers may be due to the random fluctuation of the locus of stagnation (*28, 29*). Figure 8 shows the results for local pressure and thermal transfer distribution at low free-stream turbulence. There is an indication of a small anomaly in the thermal transfer near stagnation that is symmetric with respect to the angle from stagnation. The calorimeter that was used to measure the local thermal transport and described in Figure 1 indicated low-frequency fluctuations near stagnation as well as near separation. The pressure distribution near stagnation followed accepted theory (*30*) with no anomalies. The reduction in the pressure coefficient C_P for a Reynolds number of 86,000 suggests that the boundary layer became turbulent before separation, as is expected in supercritical flow. Such behavior is also reflected in the thermal transfer results. The results compare favorably with those of Giedt (*10*) and Seban (*13*).

The introduction of the circular-hole grid patterned after Davis (*22, 23*) produced a longitudinal turbulence level of 0.135 at six mesh diameters downstream, with nearly the same scale of turbulence as the square grid used earlier (*21*). The anomaly near stagnation and the low-frequency fluctuations in thermal transfer vanished, as is shown in Figure 9. These results suggest that the apparent stagnation anomaly in thermal transfer is the result of local fluctuations near stagnation rather than turbulence anisotropy. Such fluctuations are in agreement with the turbulence amplification found near stagnation by Kuethe et al. (*29*).

Figure 10 illustrates the effects of turbulence for a Reynolds number of 22,500 on the pressure distribution and heat transfer. The effects of turbulence are larger when the pressure gradient is greater. This is to be expected from the effects of turbulence on a flat plate with a superimposed pressure gradient (*31*). The results shown in Figures 8, 9, and 10 for the circular-hole grid (*22, 23*) compare quantitatively within a few percent to those measured using a square mesh grid patterned after van der Hegge Zijnen (*21*). The turbulence influences the momentum boundary layer to a lesser degree than the thermal boundary layer, as can be seen in Figures 8, 9, and 10 from the invariance of the pressure coefficient near the forward stagnation point. The influence of Reynolds number for a level of turbulence corresponding to that of the free stream of 0.013 is shown in Figure 11, where the local Frössling number is presented as a function of the angle from stagnation with the Reynolds number as a parameter.

† Deposited as document 9341 with the American Documentation Institute, Photoduplication Service, Library of Congress, Washington 25, D. C., and may be obtained for $2.50 for photoprints or $1.75 for 35-mm. microfilm.

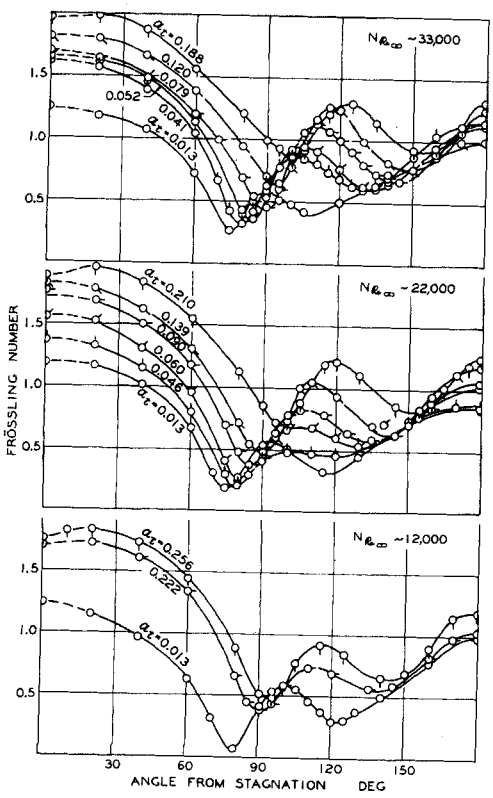

Fig. 7. Effect of level of turbulence upon local thermal transport.

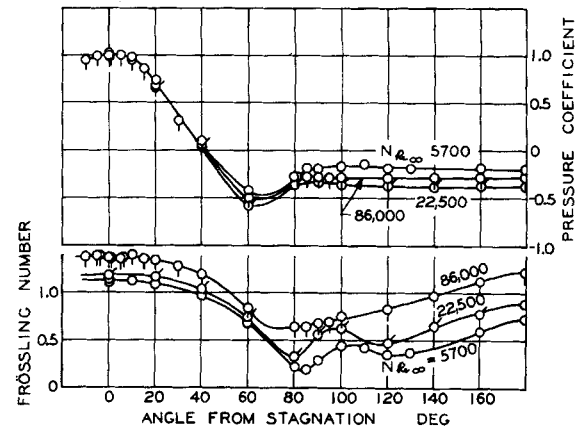

Fig. 8. Variation in Frössling number and pressure coefficient at a turbulence level of 0.013.

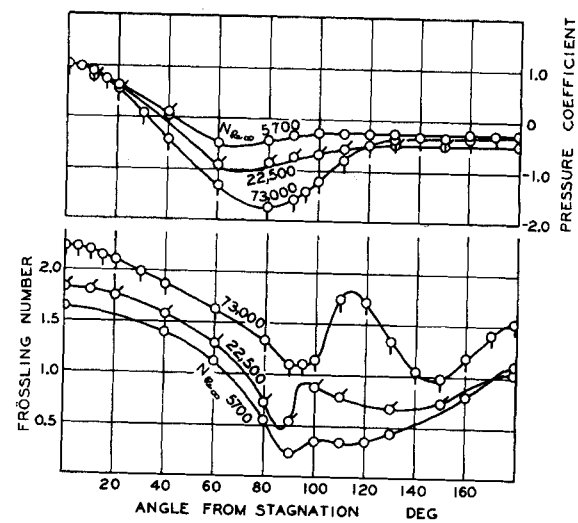

Fig. 9. Variation in Frössling number and pressure coefficient at a turbulence level of 0.135.

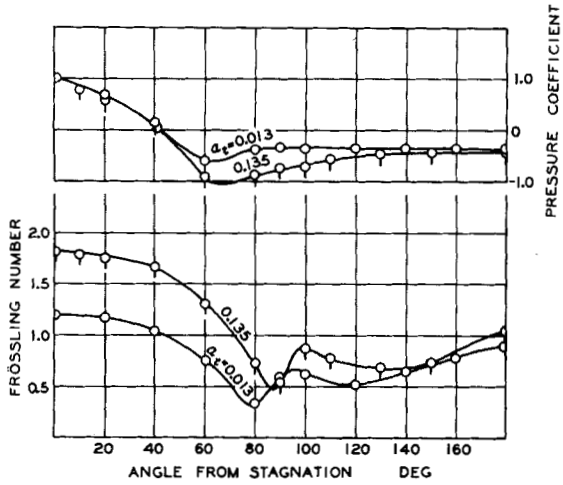

Fig. 10. Comparison of effect of turbulence level upon Frössling number and pressure coefficient at a Reynolds number of 22,500.

If Equation (5) is considered as describing the local transport at a particular angle from stagnation as a function of Reynolds number and level of turbulence, it is possible to show the behavior for the different types of flow at various positions around the cylinder. This has been done in Figure 12 where each of the four coefficients is shown as a function of angle from stagnation. The points indicated have been evaluated by nonlinear regression techniques from the experimental data† for each angle from stagnation.

The accumulated data confirm the results of earlier investigators and indicate the complicated flow pattern that exists beyond separation in the wake. In Figure 13 is shown the local Nusselt number established from the present data as a function of angle for selected Reynolds

† See footnote on page 568.

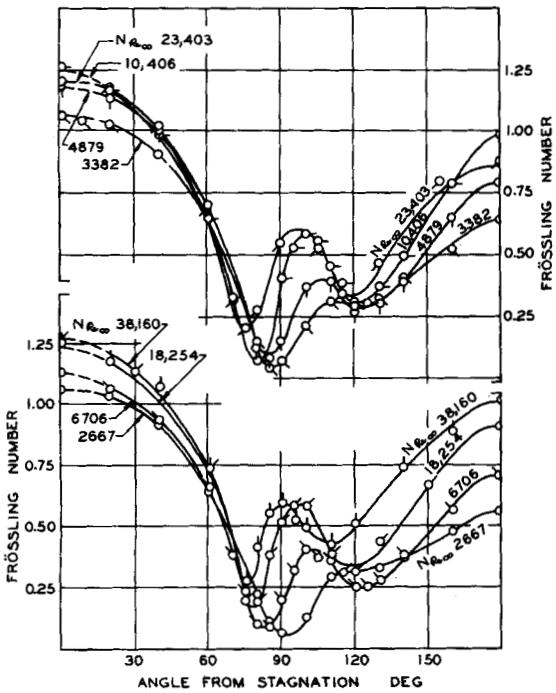

Fig. 11. Effect of Reynolds number upon local thermal transport for a turbulence level of 0.013.

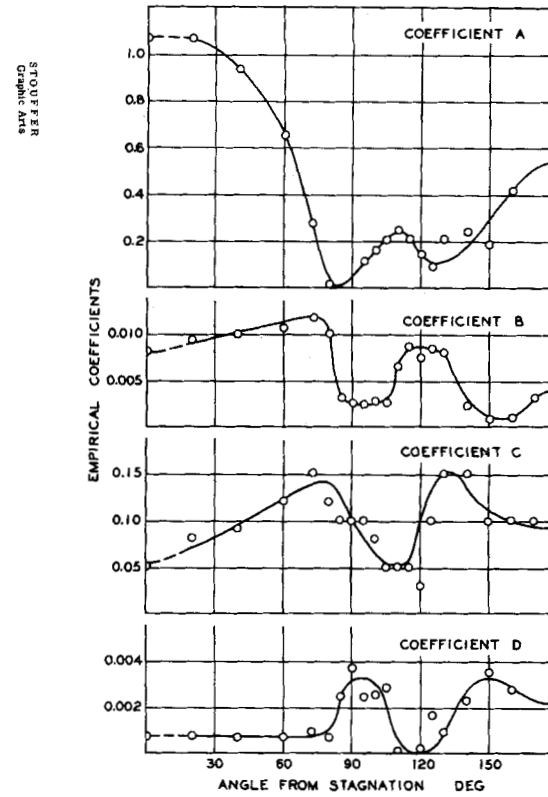

Fig. 12. Effect of angle from stagnation upon coefficients of Equation (5).

numbers for a level of longitudinal turbulence of approximately 0.013. Also included are the data of Giedt (*10*) and Seban (*13*) for a level of turbulence of 0.015.

The information available concerning local thermal transport permits an evaluation of the influence of the level of turbulence of the free stream and of Reynolds number upon the locus of the angle of separation as measured from stagnation. These results are shown in Figure 14. It is apparent that at the lower Reynolds numbers, the limited data available indicate a rather small change in

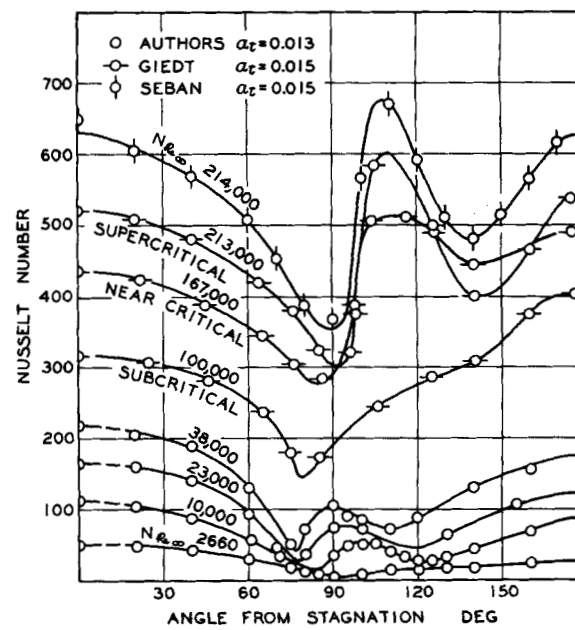

Fig. 13. Effect of angle from stagnation upon local thermal transport.

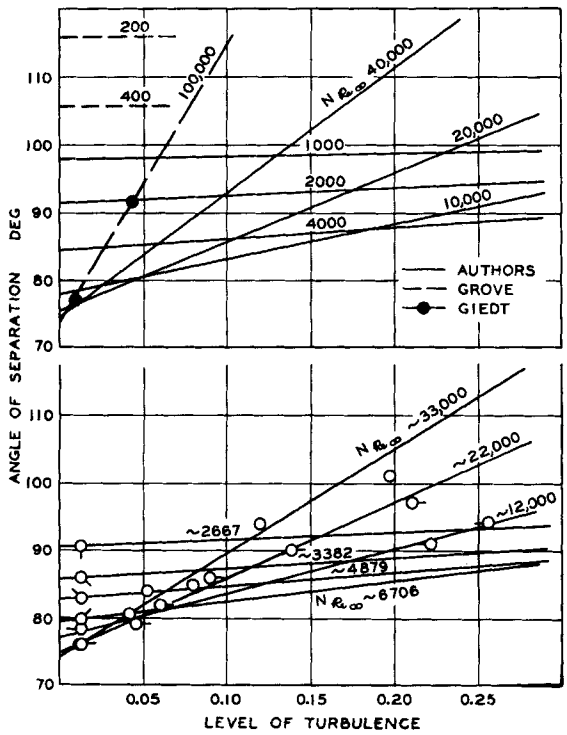

Fig. 14. Effect of flow conditions upon angle of separation.

the angle of separation with the level of turbulence of the free stream. However, at Reynolds numbers above 12,000, the angle of separation increases rapidly with an increase in the level of turbulence. Such behavior is substantiated by the measurements of Giedt (*10*) and Grove (32).

ACKNOWLEDGMENT

T. R. Galloway is a recipient of the Peter E. Fluor Memorial Fellowship and this support is gratefully acknowledged. Professor G. N. Richter assisted with the experimental program and Virginia M. Berry reviewed the calculations. June Gray prepared the figures and Grace Fitzsimons assisted with the preparation of the manuscript.

NOTATION

A, B, C, D = coefficients in Equation (5)
C_P = pressure coefficient $(P_i - P_\infty)/\frac{1}{2}(\sigma_\infty U_\infty^2)$
d = cylinder diameter, in. or ft.
h = heat transfer coefficient, B.t.u./(sec.)(sq.ft.)(°F.)
k = Frössling's coefficient in Equation (1)
k = thermal conductivity, B.t.u./(sec.)(ft.)(°F.)
N = total number of experimental data points
N_{Fs} = Frössling number, $N_{Nu}/(N_{Re}^{1/2} N_{Pr}^{1/3})$
N_{Nu} = Nusselt number, hd/k
N_{Pr} = Prandtl number, K/ν
N_{Re} = Reynolds number, dU/ν
P = pressure, lb./sq.ft.abs.
s = average deviation defined in Table 2
U_∞ = free-stream velocity, ft./sec.
u = local velocity, ft./sec.
$\overline{u'_{zf}}$ = mean longitudinal fluctuating velocity, ft./sec.

Greek Letters

α_t = level of longitudinal turbulence, fraction $[(\overline{u'_{zf}})^2]^{1/2}/U_\infty$
K = thermometric conductivity, sq.ft/sec.
ν = kinematic viscosity, sq.ft./sec.
σ' = specific weight, lb./cu.ft.
σ = standard error of estimate defined in Table 2
Σ = summation operator
ψ = angle measured from stagnation, deg.

Subscripts

e = experimental
i = evaluated at interfacial conditions
m = molecular property
p = predicted
∞ = evaluated at free-stream conditions

Superscript

* = macroscopic transport

LITERATURE CITED

1. Frössling, N., *Gerlands Beitr. Geophys.*, Band 52, Heft. 1/2, 170 (1938).
2. Goldstein, S., ed., "Modern Developments in Fluid Dynamics," Vol. II, pp. 631-632, Oxford Univ. Press (1938).
3. Squire, H. B., *ARC Rept. Mem. No. 1986* (Nov., 1942).
4. Korobkin, I., *Am. Soc. Mech. Engrs. Paper No. 54-F-18-Rev* (1954).
5. Reiher, H., *VDI Forschungsh. Gebiete Ing.*, Heft. 269 (1925).
6. Goukhman, A., V. Joukovsky, and L. G. Loiziansky, *Tech. Phys. USSR*, **1**, 221 (1934).
7. Comings, E. W., J. T. Clapp, and J. F. Taylor, *Ind. Eng. Chem.*, **40**, 1076 (1948).
8. Maisel, D. S., and T. K. Sherwood, *Chem. Eng. Progr.*, **46**, 131 (1950).
9. *Ibid.*, 172.
10. Giedt, W. H., *J. Aeronaut. Sci.*, **18**, 725 (1951).
11. Kestin, J., and P. F. Maeder, *Natl. Advisory Comm. Aeronaut. Tech. Note 4081* (1957).
12. Van der Hegge Zijnen, B. G., *Appl. Sci. Res.*, **7A**, 205 (1958).
13. Seban, R. A., *J. Heat Transfer*, **82**, 101 (1960).
14. Schnautz, J. A., Ph.D. thesis, Oregon State Coll., Corvallis (1958); Univ. Microfilm No. 33920, Ann Arbor, Mich.
15. Churchill, S. W., and J. C. Brier, *Chem. Eng. Progr. Symp. Ser. No. 17*, **51**, 57 (1955).
16. Douglas, W. J. M., and S. W. Churchill, *Chem. Eng. Progr. Symp. Ser. No. 18*, **52**, 23 (1956).
17. Perkins, H. C., Jr., and G. Leppert, *J. Heat Transfer*, **84**, 257 (1962).
18. Richardson, P. D., *Aeronaut. Res. Lab., Office Aerospace Res. USAF, AD No. 290339, ARL* 62-432 (1962).
19. Richardson, P. D., *Chem. Eng. Sci.*, **18**, 149 (1963).
20. Grafton, R. W., *ibid.*, 457 (1963).
21. Van der Hegge Zijnen, B. G., *Appl. Sci. Res.*, **A7** 149 (1957).
22. Davis, Leo, *Rept. 3-22, Jet Propulsion Lab.*, California Inst. Technol. (1950).
23. ———, *Rept. 3-17, Jet Propulsion Lab.*, California Inst. Technol. (1952).
24. Hilpert, R., *Forschungsh. Gebiete Ing.*, Pt. B, **4**, 215 (1933).
25. Couch, H. T., Ph.D. thesis, California Inst. Technol., Pasadena (1966).
26. Galloway, T. R., and B. H. Sage, "Thermal and Material Transport from Spheres. Prediction of Local Transport," California Inst. Technol., to be published.
27. ———, "Thermal and Material Transport from Spheres. Prediction of Macroscopic Thermal and Material Transport," California Inst. Technol., to be published.
28. Sutera, S. P., *J. Fluid Mech.*, **21**, 513 (1965).
29. Kuethe, A. M., W. W. Willmarth, and G. H. Crocker, "Proc. Heat Transfer Fluid Mech. Inst. *1961*," pp. 10-22, Stanford Univ. Press (1961).
30. Schlicting, Hermann, "Boundary Layer Theory," 4 ed., pp. 18-22, McGraw-Hill, New York (1960).
31. Büyüktür, A. R., J. Kestin, and P. F. Maeder, *Intern. J. Heat Mass Transfer*, **7**, 1175 (1964).
32. Grove, A. S., F. H. Shair, E. E. Petersen, and Andreas Acrivos, *J. Fluid Mech.*, **19**, 60 (1964).

Manuscript received June 9, 1966; revision received October 11, 1966; paper accepted October 11, 1966.